Carborane-Containing Liquid Crystals: Synthesis and Structural, Conformational, Thermal, and Spectroscopic Characterization of Diheptyl and Diheptynyl Derivatives of *p*-Carboranes†

Piotr Kaszynski,* Serhii Pakhomov, and Kris F. Tesh

Organic Materials Research Group, Department of Chemistry, Vanderbilt University, Nashville, Tennessee 37235

Victor G. Young, Jr.

X-ray Crystallographic Laboratory, Department of Chemistry, University of Minnesota, Minneapolis, Minnesota 55455

Received June 21, 2001

Molecular and electronic structures for four *p*-carborane derivatives were studied in the context of their liquid crystalline properties. Thus molecular and crystal structures of diheptyl and diheptynyl derivatives of 10- and 12-vertex bi-*p*-carboranes were determined by X-ray crystallography and compared to the results of ab initio calculations at the HF/6-31G* level of theory. Experimentally observed significant positional disorder of one of the substituents in the 10-vertex derivatives, **2[2]a** and **2[2]b**, was related to conformational properties of the alkyl−carborane bond. Experimental and theoretical studies of the electronic structures were conducted for the four compounds using UV and NMR spectroscopies. The nature of the unique long wavelength absorption band at 232 nm in the diheptynyl derivative **2[2]b** was explained using INDO/2//HF/6-31G* analysis. The complete assignment of the ^{13}C signals was accomplished using a long-range coupling technique and was supported by the calculated (HF/6-31G*) isotropic shielding tensors. Analysis of absorption spectra, NMR substituent effects, and trends in bond lengths shows generally strong cage−acetylene electronic interactions for the 10-vertex *p*-carborane, while the 12-vertex *p*-carborane remains largely electronically isolated. Ab initio calculations revealed that 12-vertex *p*-carborane has significantly larger electronic polarizability and quadrupole moments than the 10-vertex analogues, which are larger than those for bicyclo[2.2.2]octane compounds. All these results on packing, conformational, and electronic properties form the basis for the discussion of thermal behavior of the four carborane compounds, bicyclo[2.2.2]octane analogues, and some related compounds.

Introduction

Over the past several years we have demonstrated that *closo*-boranes are effective structural elements for liquid crystals.[1] Their unique steric and electronic molecular features offer an opportunity for the study of fundamental molecular factors imparting liquid crystalline behavior, and are also well suited for development of new electrooptical materials. Among these factors are molecular symmetry and conformational mobility and their role in stabilization of liquid crystalline phases. Small nonpolar molecular systems, such as **1**−**3** (R = alkyl) with homostructural core elements and limited conformational flexibility, are ideal for the study of these effects as well as for investigation of the role of a ring in promoting liquid crystalline behavior. Recently, we compared the mesogenic properties of two double-ring,[2] **1a** and **2a**, and single-ring[3] *p*-carborane derivatives with the analogous bicyclo[2.2.2]octane compounds **3**. Surprisingly, the derivatives of the more bulky (low aspect ratio) icosahedrane carborane **1[*n*]** exhibit much higher clearing temperatures than the analogous dialkyl derivatives of 10-vertex *p*-carborane, and this trend appears to be general for a wide range of liquid crystalline derivatives of the two *p*-carboranes.[1] The results have been attributed largely to the differences in molecular symmetries of the clusters and the conformational orientations of the substituents at the terminal positions. The difference between the cage effects on the mesogenic properties is significantly lowered, but not eliminated, in the diacetylene derivatives **1[2]b** and **2[2]b**, in which the conformational bias of the carborane−substituent junction is removed.[2] Our recent density measurements and modeling of the nematic−isotropic transition temperatures for these mesogens show a significant difference in molecular packing in the nematic phase and intermolecular interactions that affect the nematic phase stability.[4]

To provide a better understanding of the effect of molecular and electronic structures on mesogenic behavior, we examined crystal structures and spectroscopic properties for the two pairs of 12- and 10-vertex bi-*p*-carborane derivatives. Here we report

* Author for correspondence. Telephone/fax: (615) 322-3458. E-mail: PIOTR@ctrvax.vanderbilt.edu.

† Presented in part at the 215th National Meeting of the American Chemical Society, Dallas, TX, March 29−April 2, 1998. Abstr. No.: ORGN 105.

(1) Kaszynski, P.; Douglass, A. G. *J. Organomet. Chem.* **1999**, *581*, 28−38 and references therein.
(2) Czuprynski, K.; Kaszynski, P. *Liq. Cryst.* **1999**, *26*, 775−778.
(3) Douglass, A. G.; Both, B.; Kaszynski, P. *J. Mater. Chem.* **1999**, *9*, 683−686.
(4) Piecek, W.; Perkowski, P.; Kaszynski, P. Submitted for publication.

10.1021/ic010663x CCC: $20.00
Published on Web 11/06/2001

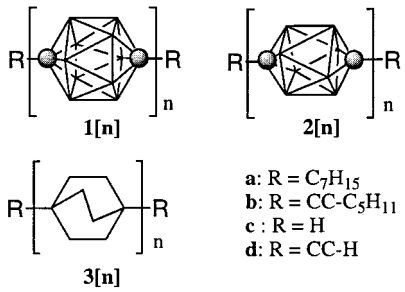

Figure 1. Derivatives of 12-vertex and 10-vertex *p*-carboranes (**1[*n*]** and **2[*n*]**) and bicyclo[2.2.2]octane (**3[*n*]**). In **1[*n*]** and **2[*n*]** each vertex corresponds to a BH fragment and the sphere represents a carbon atom.

Scheme 1

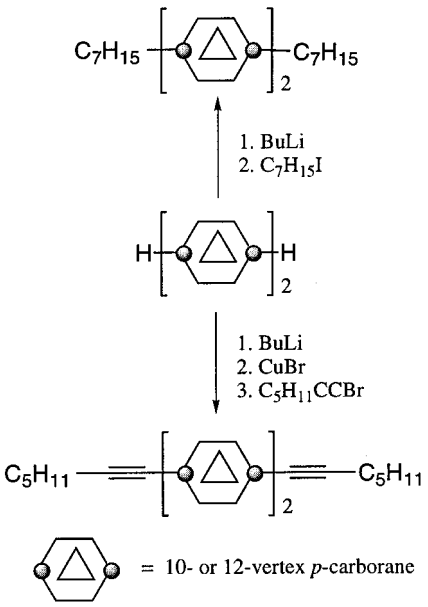

the molecular and crystal structures for **1[2]a,b** and **2[2]a,b**, their thermal behavior, and conformational and spectroscopic analyses supplemented by quantum mechanical calculations.

Results

Synthesis.

Both diheptyl and diheptynyl derivatives were prepared as shown in Scheme 1 from appropriate bi-*p*-carboranes, 1,1′-bis-(1,12-dicarba-*closo*-dodecaborane)[5] (**1[2]c**) and 1,1′-bis(1,10-dicarba-*closo*-decaborane)[6] (**2[2]c**). The dimers were converted into the corresponding dilithium salts and reacted with 1-iodoheptane to form **1[2]a** and **2[2]a**. Following a general literature procedure for icosahedron carboranes,[7] the dimers were converted to the dicopper derivatives and reacted with 1-bromo-1-heptyne to give the acetylene derivatives **1[2]b** and **2[2]b** in about 80% yield. All four compounds were purified by vacuum sublimation and recrystallization.

Crystal and Molecular Structures.

Colorless, triclinic crystals of compounds were obtained from EtOH (**1[2]a**), EtOH/CH_2Cl_2 (**1[2]b** and **2[2]b**), or pentane (**2-[2]a**) solutions, and their solid-state structures were determined by X-ray analysis. All crystals were formed under ambient conditions except for crystals of **2[2]a**, which were grown at about 4 °C. The experimental details are presented in Table 1, and selected bond lengths and angles for the four compounds are shown in Tables 2 and 3.

Table 1. Crystallographic Data

	1[2]a	**1[2]b**	**2[2]a**	**2[2]b**
chemical formula	$C_{18}H_{50}B_{20}$	$C_{18}H_{42}B_{20}$	$C_{18}H_{46}B_{16}$	$C_{18}H_{38}B_{16}$
formula weight	482.78	474.72	435.51	427.44
space group	$P\bar{1}$	$P\bar{1}$	$P\bar{1}$	$P\bar{1}$
a, Å	7.2206(2)	7.2459(5)	11.646(6)	9.4761(2)
b, Å	10.2466(2)	10.1073(7)	12.026(4)	10.4243(1)
c, Å	10.9447(4)	10.7941(8)	10.736(2)	16.1992(4)
α, deg	82.532(2)	82.853(2)	94.88(2)	78.516(1)
β, deg	72.305(2)	73.175(2)	95.72(3)	88.105(2)
γ, deg	79.744(2)	81.912(1)	101.47(1)	65.263(1)
V, Å^3	756.63(4)	746.23(9)	1457.8(9)	1421.98(5)
Z	1	1	2	2
D_{calcd}, g/cm^3	1.060	1.056	0.992	0.998
temp, K	173(2)	173(2)	193(2)	173(2)
μ,mm^{-1}	0.049	0.049	0.317	0.047
λ, Å	0.71073	0.71073	1.54178	0.71073
R^a (obsd)	0.062	0.0476	0.1423	0.0706
$R_w^{2\,b}$ (obsd)	0.1432	0.1320	0.3870	0.1773

^{a} $R = \sum||F_o| - |F_c||/\sum|F_o|$. ^{b} $R_w^2 = [\sum[w(F_o^2 - F_c^2)^2]/\sum[w(F_o^2)^2]]^{1/2}$.

12-Vertex Bicarboranes. Molecules in the crystals of **1[2]a** and **1[2]b** are located on a crystallographically imposed inversion center and are shown in Figure 2. The molecular dimensions of the bi-*p*-carborane unit are close to those obtained for the parent bi-*p*-carborane, using gas-phase electron diffraction (GED),[8] and its derivative, measured with X-ray diffraction.[9] The central C−C bond is 1.546(4) Å in **1[2]a** and 1.539(2) Å in **1[2]b**, which corresponds well to the value of 1.533(7) Å reported for a quater-*p*-carborane derivative[9] and 1.552(23) Å obtained from a GED analysis of the parent bi-*p*-carborane **1-[2]c**.[8] Incidentally, the GED value matches exactly the results of ab initio calculations for the C−C distance in **1[2]c**. The mean B−B cage edge length is 1.776 Å and ranges from 1.753 to 1.806 Å. The average intracage distances and angles in both derivatives are similar to those reported for the parent dimer[8] and are closely reproduced by ab initio calculations. A comparison of selected values is shown in Table 2.

The heptyl chains in **1[2]a** and pentyl chains in **1[2]b** adopt an almost ideal all-anti conformation with no positional disorder. They assume a pseudostaggered conformation relative to the carborane cage with the C(4)−C(3)−C(2)−B(8) dihedral angle of −14.5(3)° for the former and the C(6)−C(5)···C(2)−B(8) dihedral angle of −16.4° for **1[2]b**. This is only 3.5° or 1.6°, respectively, short of the −18° required for an ideal staggered conformation. The substituents in **1[2]a** and**1[2]b** are ideally antiperiplanar due to the presence of an inversion center.

The carborane−alkyl bond in **1[2]a** (C(2)−C(3), 1.534(3) Å) is slightly longer than a typical C−C bond (about 1.522 Å) within the alkyl chain. These distances compare well to the values of 1.541 and 1.527 Å, respectively, calculated for 1-ethyl-*p*-carborane (**4a**). The cage−acetylene bond, C(2)−C(3), in **1-[2]b** is 1.451(2) Å, which is only slightly shorter than the acetylene−alkyl distance (C(5)−C(4), 1.464(2) Å). Again, all trends and values are well reproduced by calculations for 1-butyn-1-yl-*p*-carborane (**4b**).

The unit cells of **1[2]a** and **1[2]b** contain one molecule, and the shortest separation between the long molecular axis, defined

(5) Zakharkin, L. I.; Kovredov, A. I. *Bull. Acad. Sci. USSR, Div. Chem. Sci.* **1973**, 1396.
(6) Zakharkin, L. I.; Kovredov, A. I. *Russ. J. Gen. Chem.* **1974**, *44*, 1808.
(7) Zakharkin, L. I.; Kovredov, A. I.; Olshevskaya, V. A. *Bull. Acad. Sci. USSR, Div. Chem. Sci.* **1986**, 1260−1266.
(8) Dorofeeva, O. V.; Mastryukov, V. S.; Vilkov, L. V.; Golubinskii, A. V.; Kovredov, A. I. *Russ. J. Struct. Chem.* **1989**, *29*, 942−944.
(9) Yang, X.; Jiang, W.; Knobler, C. B.; Hawthorne, M. F. *J. Am. Chem. Soc.* **1992**, *114*, 9719−9721.

Table 2. Selected Experimental and Calculated Bond Distances [Å] and Angles [deg] for 1,12-Dicarba-*closo*-dodecaborane Derivatives **1[2]a**, **1[2]b**, and Related Compounds[a]

	1[2]a	**1[2]b**	**1[2]c**			**1[2]a**	**4a**	**1[2]b**	**4b**
carborane skeleton	exptl	exptl	exptl[b]	calcd	substituents	exptl	calcd	exptl	calcd
C(1)−C(1A)	1.546 (4)	1.539 (2)	1.552 (23)	1.552	C(3)−C(2)	1.534 (3)	1.541	1.451 (2)	1.450
C(1)−B (avg)	1.726 (3)	1.721 (2)	1.736 (11)	1.735	C(4)−C(3)	1.522 (3)	1.527	1.182 (2)	1.187
B(1)−B(5) (avg)	1.783 (4)	1.778 (2)	1.795 (13)	1.791	C(5)−C(4)	1.521 (3)	na	1.464 (2)	1.473
B(1)−B(6) (avg)	1.762 (4)	1.759 (2)	1.760 (17)	1.769	C(4)−C(3)−C(2)	115.9 (2)	116.4	176.6 (2)	180.0
B(6)−B(10) (avg)	1.772 (4)	1.781 (2)	1.795 (13)	1.786	C(5)−C(4)−C(3)	112.5 (2)	na	177.7 (2)	179.3
C(2)−B (avg)	1.717 (3)	1.717 (2)	1.736 (11)	1.705	C(6)−C(5)−C(4)	113.1 (2)	na	114.08 (12)	112.6
C(1A)−C(1)−B (avg)	118.5 (2)	118.48 (13)	na	118.6	C(4)−C(3)−C(2)−B(8)	−14.5 (3)	0.0[c]	[d]	[d]
C(3)−C(2)-B (avg)	118.6 (2)	118.02 (12)	na	117.0[e]	C(5)−C(4)−C(3)−C(2)	−176.2 (2)	na	[d]	[d]
C(1)−B−B−C(2) (avg)	60.1 (2)	59.86 (12)	na	59.4	C(6)−C(5)···C(2)−B(8)	−14.4	na	−16.4	0.0[c]

[a] Experimental values are followed by results of ab initio calculations for **1[2]c**, **4a** (for substituent geometry in **1[2]a**), and **4b** (for substituent geometry in **1[2]b**). [b] Gas-phase electron diffraction data from ref 8. [c] Value set in geometry constraints. [d] Not reported. [e] The H−C−B angle.

Table 3. Selected Experimental and Calculated Bond Distances [Å] and Angles [deg] for 1,10-Dicarba-*closo*-decaborane Derivatives **2[2]a**, **2[2]b**, and Related Compounds[a]

	2[2]a	**2[2]b**	**2[2]c**		**2[2]a**	**5a**	**2[2]b**	**5b**
carborane skeleton	exptl[b]	exptl[c]	calcd	substituents	exptl[b]	calcd	exptl[c]	calcd
C(1)−C(10)	1.461 (10)	1.488 (3)	1.498	C(3)−C(2)	1.513 (11)	1.524	1.445 (4)	1.440
C(1)−B (avg)	1.607 (12)	1.604 (4)	1.605	C(4)−C(3)	1.516 (11)	1.528	1.188 (3)	1.1875
B(1)−B(4) (avg)	1.83 (2)	1.844 (4)	1.858	C(5)−C(4)	1.498 (11)	na	1.458 (4)	1.473
B(1)−B(5) (avg)	1.80 (2)	1.805 (4)	1.825	C(4)−C(3)−C(2)	114.0 (7)	115.2	178.1 (3)	179.9
B(5)−B(8) (avg)	1.81 (2)	1.850 (4)	1.861	C(5)−C(4)−C(3)	113.4 (7)	na	178.4 (3)	179.4
C(2)−B (avg)	1.595 (13)	1.612 (4)	1.596	C(6)−C(5)−C(4)	113.5 (7)	na	114.2 (3)	112.7
C(10)−C(1)-B (avg)	126.6 (8)	125.6 (2)	125.1	C(4)−C(3)−C(2)−B(6)	−25.2 (14)	0.0[d]	[e]	[e]
C(3)−C(2)−B (avg)	126.6 (7)	125.7 (2)	124.4	C(13)−C(12)−C(11)−B(14)	−18 (3)	0.0[d]	[e]	[e]
B−C(1)− C(10)−B (avg)	45.0 (13)	45.0 (4)	45.0[d]	C(13′)−C(12′)−C(11)−B(14)	−49.0 (2)	0.0[d]	[e]	[e]
C(1)−B−B−C(2) (avg)	76.4 (9)	75.6 (3)	74.5[f]	C(5)−C(4)−C(3)−C(2)	−173.8 (8)	na	[e]	[e]
				C(6)−C(5)···C(2)−B(X)	−9.4 (X = 6)	na	−19.6 (X = 8)[g]	0.0[d]

[a] Experimental values are followed by results of ab initio calculations for **2[2]c**, **5a** (for substituent geometry in **2[2]a**), and **5b** (for substituent geometry in **2[2]b**). [b] Values for the nondisordered cage. [c] Average values for two carborane cages. [d] Value set in geometry constraints. [e] Not reported. [f] The H−C−B angle. [g] The angle C(15)−C(14)···C(11)−B(13) is −31.6°.

as being coincidental with the C(1)−C(1A) bond, is about 6.1 Å for the crystal of **1[2]a** and 5.3 Å in the crystal of **1[2]b**. The closest contact of 2.29 Å is observed between B(3)H and B(3A)H in the crystal of **1[2]b**.

10-Vertex Bi-*p*-carboranes. Compounds **2[2]a** and **2[2]b** provide the first examples of structurally characterized 10-vertex bi-*p*-carboranes, and their molecular structures are shown in Figure 3. The intercage bonds are 1.461(10) and 1.488(3) Å, respectively, which are significantly shorter than the analogous bond in the 12-vertex analogue. The intracage C−B and B−B distances are typical for the parent *p*-carborane[10] **2[1]c**, and all favorably compare to the calculated values as shown in Table 3. In both compounds, the *p*-carborane cages are staggered with the average dihedral angle indistinguishable from the ideal 45°.

One of the two alkyl chains in **2[2]a** is significantly disordered. The alkyl chain without positional disorder adopts an almost ideal all-anti conformation with the largest deviation of about 6° from the ideal 180° for the orientation of substituents around the C(3)−C(4) and C(4)−C(5) bonds. In contrast, the chain disordered over two positions adopts a gauche orientation for the $C_\beta-C_\gamma$ in one chain and $C_\delta-C_\epsilon$ bonds in the other. The nondisordered chain forms a pseudostaggered conformation with respect to the carborane cage with a dihedral angle C(4)−C(3)−C(2)−B(6) of −25.2(14)°. The analogous values for the disordered chain are −18(3)°, for C(13)−C(12)−C(11)−B(14), and −49(2)°, for C(13′)−C(12′)−C(11)−B(14). This gives the angles between the plane of one alkyl chain (C(4)−C(3)−C(2)) and the two positional occupancies for the disordered chain of 29° (C′(13)−C′(12)−C′(11) plane) and 4° (C(13)−C(12)−C(11) plane).

Similarly, one of the heptynyl chains in **2[2]b** shows positional disorder of the terminal propyl group C(7)−C(8)−C(9) over two sites. The more probable orientation of the propyl group is trans with respect to the rest of the alkyl chain (C(6)−C(7)−C(8)−C(9), 176.7(7)°), while the less probable orientation of the alkyl chain is close to a gauche conformation (C(6)−C(7)−C(8′)−C(9′), −80(2)°). The angle between the alkyl chain planes defined as C(6)−C(5)···C(2) and C(11)···C(14)−C(15) is 85°.

The alkyl−carborane C(2)−C(3) distance in **2[2]a** is 1.513(11) Å, while the acetylene−cage bond in **2[2]b** is 1.445(4) Å.

The unit cell of **2[2]a** and **2[2]b** contains a pair of conformational enantiomers related by an inversion center and oriented antiparallel to each other. The intermolecular distance between the long molecular axes, defined as being coincidental with the C(1)−C(10) bond, is about 5.2 Å in both crystals.

Conformational Analysis.

The conformational potential energy surface for the heptyl derivatives **1[2]a** and **2[2]a** was inferred from results of ab initio calculations for staggered and eclipsed conformations of smaller molecular fragments: parent bi-p-carboranes **1[2]c** and **2[2]c** and 1-ethyl-*p*-carboranes **4a** and **5a**. The conformational potential energy surface for the acetylene substituent in **1[2]b** and **2[2]b** was assumed to be flat. The results are shown in Table 4.

As expected, calculations show that the staggered bi-p-carboranes represent the conformational minimum (Figure 4), while the eclipsed conformers correspond to conformational maxima. The height of the barrier to internal rotation is substantial for

(10) Atavin, E. G.; Mastryukov, V. S.; Golubinskii A, V.; Vilkov, L. V. *J. Mol. Struct.* **1980**, *65*, 259−269.

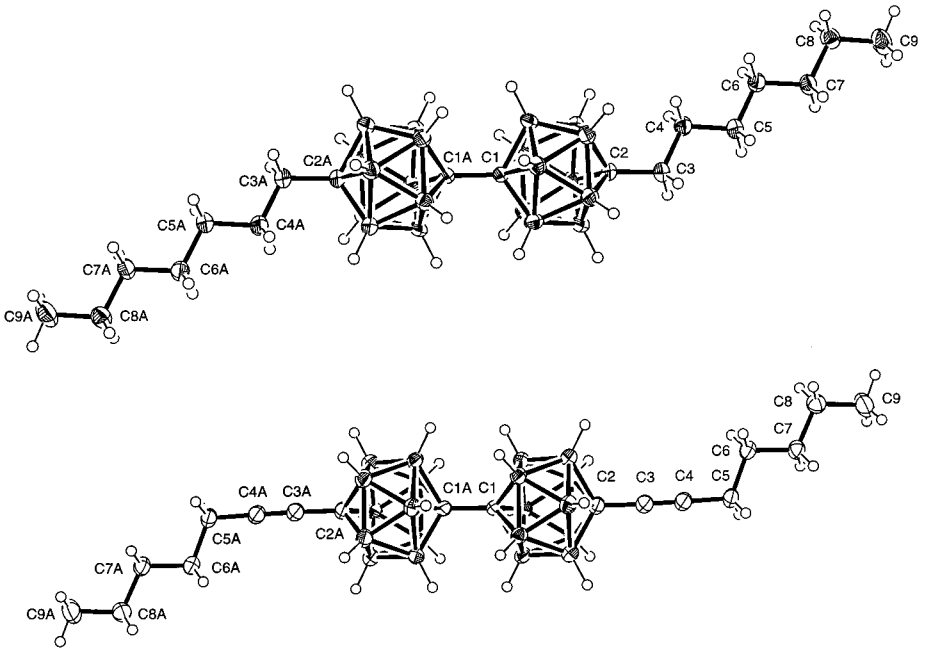

Figure 2. Thermal ellipsoid diagrams of (a) 1,1′-bis[12-heptyl-1,12-dicarba-*closo*-dodecaborane] (**1[2]a**) and (b) 1,1′-bis[12-hept-1-ynyl-1,12-dicarba-*closo*-dodecaborane] (**1[2]b**) drawn at 50% probability.

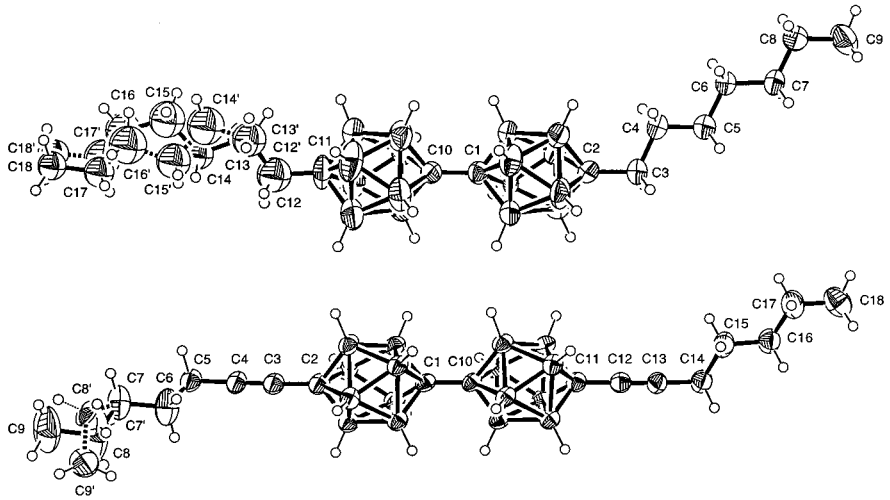

Figure 3. Thermal ellipsoid diagrams of (a) 1,1′-bis[10-heptyl-1,10-dicarba-*closo*-decaborane] (**2[2]a**) and (b) 1,1′-bis[10-hept-1-ynyl-1,10-dicarba-*closo*-decaborane] (**2[2]b**) drawn at 50% probability.

Table 4. Calculated (HF/6-31G*) Enthalpy and Free Energy Differences between Conformational Extremes in Dimers **1[2]c**, **2[2]c**, and **3[2]c**, and 1-Ethyl Derivatives **4a**, **5a**, and **6a**[a]

	$\mathcal{A}$ = *p*-$C_2B_{10}H_{11,}$ **1**		$\mathcal{A}$ = *p*-$C_2B_8H_{9,}$ **2**		$\mathcal{A}$ = 1,4-$C_8H_{13,}$ **3**	
	ΔH_{298}	ΔG_{298}	ΔH_{298}	ΔG_{298}	ΔH_{298}	ΔG_{298}
$\mathcal{A}-\mathcal{A}$[b]	7.74	8.90	3.14	4.84	9.09	10.13
$\mathcal{A}$−Et[c]	0.12	1.32	0.45	1.62	4.33[b]	3.89[b]

[a] Energy in kcal/mol. [b] Difference between the eclipsed and staggered conformations. [c] Difference between the staggered and eclipsed conformations.

the 12-vertex bi-p-carborane **1[2]c** (8.9 kcal/mol) and smaller (4.8 kcal/mol) for the 10-vertex analogue **2[2]c**.

The conformational potential energy surface for 1-ethyl-*p*-carboranes **4a** and **5a** exhibits a shallow minimum of about 1.5 kcal/mol for the eclipsed form.

Thermal Properties.

As we reported earlier,[2] the diheptyl derivatives **1[2]a** and **2[2]a** form narrow temperature range nematic phases, while the diheptynyl derivatives **1[2]b** and **2[2]b** are nonmesogenic. Studies of binary mixtures of **1[2]b** and **2[2]b** with a nematic host permitted the extrapolation of the virtual nematic−isotropic transition temperatures. They were found to be more than 120 °C below their melting temperatures or more than 150 °C below the isotropic transition for their diheptyl analogues. For comparison the melting temperatures and enthalpies for the parent bi-p-carboranes **1[2]c** and **2[2]c** have been also measured and are listed in Table 5.

Three out of four derivatives were found to form crystalline polymorphs. The 10-vertex diheptyl derivative **2[2]a** undergoes two low-energy Cr−Cr transitions, first at −116 °C and second

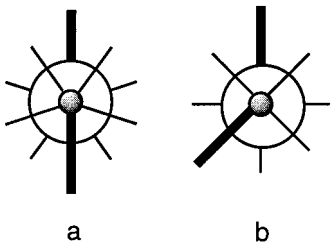

Figure 4. Extended Newman projection along the long molecular axes of (a) the 12-vertex and (b) the 10-vertex derivatives **1[*n*]a** and **2[*n*]a**. The bar represents the alkyl substituent plane.

Table 5. Transition Temperatures [°C] and Enthalpies [kJ/mol][a]

compound		Cr1	Cr2	S	N	I
1[2]a	*T*/Δ*H*	• 92.2/21	• 143.3/22		• 148.2/1.1	•
2[2]a	*T*/Δ*H*	• 19.9/2.5[b]	•82.3/26		(• 82.5/1.6)[c]	•
3[2]a[d,e]	*T*	• 47		• 226		•
1[2]b	*T*/Δ*H*	• 93.8	• 96.3/37[f]		[• −31][g]	•
2[2]b	*T*/Δ*H*	• 77.1/25			[• −73][g]	•
1[1]c	*T*	• 259−261[h]				•
2[1]c	*T*	• 161−162[i]				•
3[1]c	*T*	• 174−175[j]				•
1[2]c	*T*	• 355				•
2[2]c	*T*	• 173				•
3[2]c	*T*	• 234−236[k]				•

[a] Observed phases are denoted by bullets and the monotropic transition is in parentheses. Cr, crystal; S, smectic; N nematic; I, isotropic. Some of the data are taken from ref 2. [b] An additional Cr−Cr transition was observed at −116 °C (0.4 kJ/mol). [c] Monotropic transition. [d] Reference 14. [e] Unidentified smectic phases. Enthalpies not reported. [f] Total enthalpy of melting. [g] Virtual transition temperatures were obtained in 1-(4-pentylbicyclo[2.2.2]oct-1-yl)-2-(4-methoxyphenyl)ethane (ref 2). [h] Papetti, S. Heying, T. L. *J. Am. Chem. Soc.* **1964**, *86*, 2259. [i] Garret, P. M.; Smart, J. C.; Ditta, G. S.; Hawthorne, M. F. *Inorg. Chem.* **1969**, *8*, 1907. [j] Doering, W. von E.; Farber, M.; Sprecher, M.; Wiberg, K. B. *J. Am. Chem. Soc.* **1952**, *74*, 3000; [k] Adcock, W.; Iyer, V. S. *J. Org. Chem.* **1988**, *53*, 5259.

at 20 °C. The 12-vertex analogue exhibits only one such transition at 92 °C. In contrast to the 10-vertex derivative, the Cr−Cr transition in **1[2]a** is sharp and involves a relatively large change of enthalpy. The thermal behavior of the 12-vertex diheptynyl derivative **1[2]b** is most curious. The thermal and optical analysis of **1[2]b** revealed that the natural polymorph obtained from crystallization melts at 93.8 °C. Upon continuous heating, the liquid subsequently crystallizes and the resulting second polymorph melts at 96.3 °C.

Both acetylene derivatives **1[2]b** and **2[2]b** are thermally stable under nitrogen up to at least 300 °C.

In all three series of compounds listed in Table 5, the 10-vertex derivatives melt at temperatures lower than those for the 12-vertex analogues. This is also reflected in significantly lower nematic−isotropic transition temperatures (T_i) in the pairs of the diheptyl and diheptynyl derivatives. The largest difference in the melting point temperatures (about 180 °C) is observed for the parent bi-*p*-carboranes **1[2]c** and **2[2]c**.

Spectroscopy. Electronic Absorption Spectroscopy. Electronic absorption spectra of the heptynyl carborane derivatives revealed significant electronic interactions between 10-vertex *p*-carborane and the acetylene substituent, which are absent in the 12-vertex analogue **1[2]b**. While the absorption band at 193 nm of 12-vertex heptyl carborane derivative **1[2]a** is unaffected by substitution with acetylene in **1[2]b**, a strong absorption at 200 nm exhibited by the 10-vertex analogue **2[2]a** appears to be red-shifted to 232 nm upon substitution with acetylene in **2[2]b** (Figure 5).

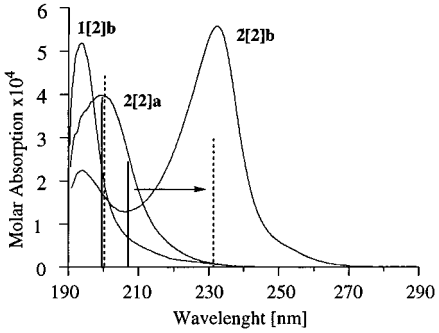

Figure 5. Electronic absorption spectra for selected compounds recorded in MeCN. Vertical lines represent the ZINDO calculated major transitions for **2[2]c** (solid lines) and **2[2]d** (dashed lines). Oscillator strength values scaled by 8.1×10^4.

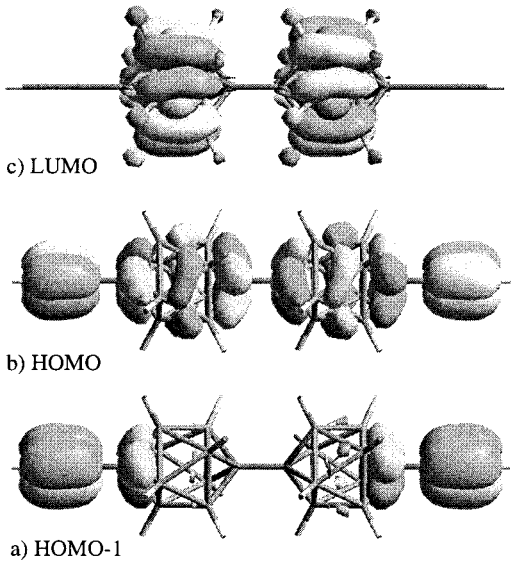

Figure 6. Representation of molecular orbitals calculated (INDO/2//HF/6-31G*) for **2[2]d**: (a) HOMO-1, (b) HOMO, and (c) LUMO.

To shed more light on the nature of the observed electronic interactions, we performed ZINDO calculation at the HF/6-31G* geometries. An analysis of the computational results for 10-vertex bi-*p*-carborane **2[2]c** suggests that the broad absorption band observed at 200 nm for **2[2]a** is composed of two bands calculated at 199 and 207 nm. The first band represents a combination of HOMO-2−LUMO and HOMO-1−LUMO+1 electronic transitions with a diagonal transition dipole of 3.2 D. The low-energy band results from the HOMO−LUMO electronic transition with a longitudinal transition dipole of 3.6 D. Substitution of acetylene at the carbon atoms in bi-*p*-carborane and electronic interactions in the resulting diethynyl-bi-*p*-carborane (**2[2]d**) lead to increasing energy for the HOMO and formation of an additional high-lying MO. In consequence, the two highest occupied orbitals in **2[2]d** include the acetylene subunit, while the two lowest unoccupied MOs (LUMO and LUMO+1) and two lower occupied orbitals (HOMO-2 and HOMO-3) involve only the bi-*p*-carborane σ electron manifold. A graphical reperesentation of three of these orbitals is shown in Figure 6.

Based on the ZINDO results, the long wavelength absorption observed for **2[2]b** at 232 nm and calculated for **2[2]d** at 231 nm is a combination of symmetry-allowed HOMO−LUMO and HOMO-1−LUMO+1 electronic transitions with the longitudinal transition dipole of 4.2 D. The second band at 193 nm in **2[2]b** (calculated for **2[2]d** at 200 nm) presumably results from

Table 6. Experimental[a] and Calculated[b] ^{11}B and ^{13}C NMR Data for **1[2]** and **2[2]** Derivatives

	C(12)	B(7-11)	B(2-6)	C(1)
1[2]a[c]	83.0 (82.8)	−14.4 (−14.7)	−13.3 (−13.2)	78.3 (80.2)
1[2]b[c,d]	68.5 (68.2)	−13.5 (−13.5)	−13.5 (−13.6)	79.0 (79.3)
1[2]c[e]	61.7 (63.9)	−16.8 (−16.9)	−13.1(−12.9)	83.7 (83.7)
	61.7[f]	−15.8[g]	−13.1[g]	83.9[f]
1[1]c	63.6	−15.9	−15.9	63.6
	63.6[h]	−15.8[g]	−15.8[g]	63.6[h]

	C(10)	B(6-9)	B(2-5)	C(1)
2[2]a[c]	121.5 (120.6)	−12.1 (−12.1)	−10.3 (−10.6)	112.6 (113.7)
2[2]b[c,i]	102.2 (102.8)	−10.6 (−10.5)	−10.6 (−10.7)	114.7 (116.3)
2[2]c[e]	97.8 (100.6)	−13.8 (−13.8)	−9.9 (−10.1)	120.6 (118.6)
		−13.7[g]	−9.8[g]	
2[1]c	101.8	−13.7	−13.7	101.8
	102.3[h]	−13.8[g]	−13.8[g]	102.3[h]

[a] Chemical shifts in ppm obtained in $CDCl_3$ relative to $B(OMe)_3$ (18.1 ppm). [b] The HF/6-31G*−GIAO-predicted values, as a sum of the substituent effect on the chemical shift of the parent carboranes **1[1]c** and **2[1]c**, are shown in parentheses. See text for details. For the complete list of calculated absolute isotropic shielding tensor, see Supporting Information. [c] Connectivity obtained from the HMBC experiment. [d] Chemical shifts for the ethynyl fragment: C_α, 75.9; C_β, 83.0 ppm. [e] Obtained from a DEPT-135 experiment. [f] Spectrum recorded in benzene (ref 9). [g] Reference 13. [h] Fedin, E. I.; Antonovich, V. A.; Rys, E. G.; Kalinin, V. N.; Zakharkin, L. I. *Bull. Acad. Sci. USSR, Chem. Div.* **1975**, 723. [i] Chemical shifts for the ethynyl fragment: C_α, 77.0; C_β, 87.6 ppm.

HOMO-3−LUMO and HOMO-2−LUMO + 1 excitations with a transverse transition dipole of 3.5 D. These transitions are little affected by the substitution of the parent bi-*p*-carborane (**2[2]c**) with acetylene and only slightly red-shifted by 1 nm, according to the calculations.

A similar analysis for the 12-vertex carborane analogues **1-[2]d** showed no electronic interaction between the carborane and the acetylene substituent, revealing them as separate electronic systems. These results are qualitatively identical with those obtained for carborane dicarbonitriles and diacetylenes.[11,12]

NMR Spectroscopy. The electronic effects observed in the UV spectra are also reflected in the NMR chemical shifts listed in Table 6 especially in the ^{13}C NMR spectra. The ^{13}C NMR signals for the cage atoms and acetylene subunits were assigned using DEPT-135 (for **1[2]c** and **2[2]c**) and a long-range ^{1}H−^{13}C coupling technique (HMBC) for their derivatives. The ^{11}B NMR signals were assigned based on general trends.[13] The assignment of experimental chemical shifts was further supported by the results of ab initio calculations in which the values were derived in the following way: (a) the chemical shift increments (CSI) for the carborane, ethyl, and butynyl substituents were derived by comparison of isotropic shielding tensors (IST) for the bi-*p*-carborane, 1-ethyl-*p*-carborane, and 1-butyn-1-yl-*p*-carborane with those IST for the corresponding parent carboranes **1[1]c** and **2[1]c** (Table 7); (b) the resulting CSI were added to the experimental ^{13}C and ^{11}B NMR chemical shifts of the parent carboranes **[1]c**. The theoretical CSI are listed in Table 7, and the experimental and computed chemical shifts are compared in Table 6.

The experimental chemical shifts are in excellent agreement with the computational results as is apparent from the data in Table 6. A statistical analysis of the differences between the experimental and calculated values shows small mean difference and standard deviations (STD). Thus for ^{13}C, the mean difference is −0.6 ppm and STD = 1.4 ppm, while the same values for the ^{11}B nucleus are 0.06 and 0.16 ppm. More extensive NMR correlation studies for *p*-carboranes will be reported elsewhere.

Table 7. Calculated ^{13}C and ^{11}B NMR Chemical Shift Increments (CSI) $\Delta\delta$ for Derivatives of *p*-Carboranes[a]

	^{13}C $\Delta\delta$		^{11}B[b] $\Delta\delta$	
1-X-*p*-$C_2B_{10}H_{11}$	C(1)	C(12)	B(2-6)	B(7-11)
X = H	0.0	0.0	0.0	0.0
X = *p*-$C_2B_{10}H_{11}$	+20.1	+0.3	+3.0	−1.0
X = $-CH_2CH_3$	+18.9	−3.5	+2.2	−0.3
X = $-C{\equiv}C-CH_2CH_3$	+4.0	−2.3	+3.4	−0.7

	^{13}C $\Delta\delta$		^{11}B[b] $\Delta\delta$	
1-X-*p*-$C_2B_8H_9$	C(1)	C(10)	B(2-5)	B(6-9)
X = H	0.0	0.0	0.0	0.0
X = *p*-$C_2B_8H_9$	+16.8	−1.2	+3.6	−0.1
X = $-CH_2CH_3$	+20.0	−4.9	+1.7	−0.5
X = $-C{\equiv}C-CH_2CH_3$	+2.2	−2.3	+3.3	−0.6

[a] Obtained from comparison of the HF/6-31G*−GIAO-derived isotropic chemical shifts in ppm with those calculated for the parent carboranes. See text for details. [b] Average calculated value.

Table 8. Chemical Shifts δ and Chemical Shift Increments $\Delta\delta$ for Selected Derivatives of 1-Hexyne, X−C(1)≡C(2)−C_4H_9

	δ		$\Delta\delta$	
X	C(1)	C(2)	C(1)	C(2)
H[a]	68.2	84.6	0	0
$C_2H_{11}B_{10}$[b]	75.9	83.0	+7.7	−1.6
$C_2H_9B_8$[c]	77.0	87.6	+8.8	+3.0
Me[a]	75.3	79.4	+7.1	−5.2
Ph[d]	80.6	90.6	+12.4	+6.0
MeCO[e]	81.6	91.2	+13.4	+6.6

[a] Poleschner, H.; Heydenreich, M. *Magn. Reson. Chem.* **1995**, *33*, 917. [b] Chemical shifts for **1[2]b**. The effect of the second cage and the chain length difference is neglected. [c] Chemical shifts for **2[2]b**. The effect of the second cage and the chain length difference is neglected. [d] Crisp, G. T.; Turner, P. D.; Stephens, K. A. *J. Organomet. Chem.* **1998**, *570*, 219. [e] Kalabin, G. A.; Proidakov, A. G.; Gavrilov, L. D.; Vereshchagin, L. I. *J. Org. Chem. USSR* **1977**, *13*, 449.

Inspection of the theoretical CSI listed in Table 7 shows generally stronger substituent antipodal effects in 10-vertex carborane derivatives than in the 12-vertex analogues. For instance, introduction of an alkyl group into **2[1]c** results in a significant shielding of the antipodal C(10) carbon by −4.9 ppm, while for the 12-vertex analogue **1[1]c** the effect is smaller, about −3.5 ppm. Substitution of an alkynyl group into the carborane increases the shielding of the antipodal carbon to a similar extent in both carboranes, by −2.3 ppm. A significant (about +19 ppm) and modest (about +2 and +4 ppm) deshielding of the ipso carbon in both carboranes is caused by the alkyl and alkynyl groups, respectively.

Interesting results were obtained from a comparison of the effect of the carborane cage on the acetylene ^{13}C chemical shifts in 1-hexyne with other substituents as shown in Table 8. While the effect of the 12-vertex carborane on acetylene is comparable to that of the methyl substituent, the effect of the 10-vertex cage is more reminiscent of that of a phenyl group.

A similar trend is observed for the protons of the CH_2 group attached directly to the cage. In the 12-vertex carborane **1[2]a** the methylene protons absorb at about 1.50 ppm, while in the

(11) Pakhomov, S.; Kaszynski, P.; Young, V. G., Jr. Unpublished results.
(12) Pakhomov, S.; Kaszynski, P.; Young, V. G., Jr. *Inorg. Chem.* **2000**, *39*, 2243−2245.
(13) Müller, J.; Baše, K.; Magnera, T.; Michl, J. *J. Am. Chem. Soc.* **1992**, *114*, 9721−9722.

10-vertex analogue **2[2]a** the nuclei are significantly deshielded and the resonance appears at 3.23 ppm. This correlates well with the ^{13}C NMR chemical shift of the cage carbon atoms which appear in the "sp^2 region" of the spectrum (about 110 ppm) for the 10-vertex and are shifted upfield by about 40 ppm in the 12-vertex analogues.

Discussion and Conclusions

Crystallographic results are consistent with the suggestion that the observed differences in the melting and clearing points in the two heptyl derivatives **1[2]a** and **2[2]a** are related to their conformational properties.[3] While molecules of the higher melting and clearing 12-vertex derivatives favor the most elongated antiperiplanar conformational minima in their solid-state structures, substituents in the lower clearing 10-vertex analogues are not coplanar and exhibit gauche conformations with a significant positional disorder in the solid state. The observed solid-state structures originate from the distribution of conformational minima in derivatives of both carboranes. The C_{5d} symmetry of the 12-vertex *p*-carborane **1[1]c** allows for a conformational minimum of **1[*n*]a** with antiperiplanar alkyl chains, while the chains in **2[*n*]a** are offset from coplanarity by 45°, forming chiral conformers (Figure 4). The orientation of the alkyl chains relative to the carborane cage in the crystal structures of **1[2]a** and **2[2]a** differs from the results of ab initio calculations, which predict eclipsed conformational minima for both derivatives. This is not surprising, considering that the minima for both alkyl carboranes are shallow and the calculated enthalpy difference between the eclipsed and staggered forms is less than 0.5 kcal/mol (Table 4). The corresponding free energy difference is greater, close to 1.5 kcal/mol, and defines the gas-phase dynamic distribution of alkyl chain orientations with respect to the cage.

The role of conformational effects on mesophase stability is also consistent with the results obtained for the single-ring derivatives **1[1]** and **2[1]** ($R = C_5H_{11}$).[3] Molecules of the latter compound are bent in their conformational minima closer to their molecular centers, which results in lower shape anisotropy and larger destabilization of the nematic phase relative to the two-ring analogue **2[2]a**. Consequently, the difference in virtual nematic−isotropic temperatures [T_i] increases from about 65 °C in the **1[2]a** and **2[2]a** pair to close to 90 °C in the single-ring compounds. Removing the conformational bias in **1[2]a** and **2[2]a** by replacing the $-CH_2CH_2-$ unit with an acetylene fragment in **1[2]b** and **2[2]b** lowers the difference in [T_i] to about 40 °C in favor of the 12-vertex. Surprisingly, this structural change also depresses the nematic−isotropic transition by over 150 °C in each compound.

The observed dramatic destabilization of the nematic phase in **1[2]b** and **2[2]b** relative to **1[2]a** and **2[2]a** results, presumably, from virtually free rotation of the heptynyl substituents in the former and hence their low dynamic molecular aspect ratio in the condensed phase. On the other hand, a significant barrier to intramolecular rotation around the heptyl-bridgehead carbon in bicyclo[2.2.2]octane derivative **3[2]a** (Table 4) results in conformational rigidity and a high dynamic aspect ratio for **3[2]a** in the condensed phase. This coincides with a high clearing temperature of 226 °C[14] observed for **3[2]a** (Table 5). These observations are consistent with findings for other compounds and a suggestion that increased conformational mobility and substituent flexibility is detrimental to the mesophase stability.[15]

The difference in the nematic phase stability of carborane derivatives, even in the acetylene derivatives with free internal rotation, is also reflected in the significant difference in melting point temperatures, by about 180 °C, of the parent carboranes **1[*n*]c** and **2[*n*]c** (Table 5). Although the low melting point of **2[2]c** can be ascribed, in part, to the lower barrier to internal rotation around the carborane−carborane C−C bond (Table 4), it cannot explain such a large difference in melting points. These results demonstrate that the conformational effects cannot be solely responsible for the generally higher melting and clearing temperatures observed in the 12-vertex derivatives.[1]

Experiments and calculations show significant differences in the electronic properties of the two *p*-carboranes and consequently in their interactions with substituents. While UV absorption spectra, substituent effects in ^{13}C NMR spectroscopy, and molecular structure data clearly show strong cage−substituent interactions in the 10-vertex derivatives, the 12-vertex carborane remains largely electronically isolated. Despite the very similar hybridization used by the carborane carbon atom to form the exocyclic bond to the substituent ($sp^{1.91}$ in **1[1]c** and $sp^{1.96}$ in **2[1]c**), the 10-vertex carborane has all the characteristics of being an sp^2-type substituent, while the 12-vertex *p*-carborane behaves like an sp^3-type substituent in its derivatives. This is reflected in the electronic absorption spectra of π derivatives, e.g., **2[2]b** in Figure 5, chemical shifts of the cage carbon atoms, and their sensitivity to substituent effects. The sp^2 character of the 10-vertex carborane is also apparent from the experimental and calculated bond lengths in the heptyl **1[2]a** and **2[2]a**, acetylene **1[2]b** and **2[2]b**, and other derivatives.[12,16] For instance, the $C_{cage}-C_{alkyl}$ bond in **1[2]a** (1.534(2) Å) is close to a mean alkyl−alkyl distance (1.530(15) Å), while in **2[2]a** (1.513(11) Å) it is closer to that of a mean vinylalkyl bond length (1.507(15) A).[17] Similarly, the acetylene $C_{cage}-C_{\equiv}$ bond in **1[2]b** (1.451(2) Å) is similar for alkylacetylenes (1.466(10) Å), while in **2[2]b** (1.445(2) Å) it is more characteristic for vinylacetylenes (1.431(14) Å).[17] Although the difference in bond lengths between **1[2]b** and **2[2]b** is crystallographically insignificant, the trend and the values are well reproduced by ab initio calculations (Tables 2 and 3).

Computational analysis of the electronic structures for parent carboranes and their derivatives shows that, despite greater electronic intramolecular interactions in the 10-vertex compounds, the 12-vertex analogues have significantly larger average electronic polarizabilities α_{avg} (Table 9). Derivatives of the 10-vertex *p*-carborane show, however, slightly higher anisotropy of electronic polarizability $\Delta\alpha$ and, consequently, higher $\Delta\alpha/\alpha_{avg}$ ratios[2] which are proportional to the ratio of anisotropic to isotropic potentials L_2/L_0 in the van der Waals theory of the nematic state.[18,19] This leads to the expectation that 10-vertex derivatives should have transition temperatures higher than, or at least similar to, those of the 12-vertex analogues. Experiments show the contrary.

(14) Reiffenrath, V.; Schneider, F. *Z. Naturforsch. A* **1981**, *36a*, 1006−1008.

(15) Deutscher, H. J.; Frach, R.; Tschierske, C.; Zaschke, H. In *Selected Topics in Liquid Crystal Research*; Koswig, H.-D., Ed.; Akademie-Verlag: Berlin, 1990; pp 1−18, and references therein.

(16) Kaszynski, P. In *Anisotropic Organic Materials*; Glaser, R., Kaszynski, P., Eds.; ACS Symposium Series 798; American Chemical Society: Washington, DC, 2001; pp 68−82.

(17) Allen, F. H.; Kennard, O.; Watson, D. G.; Brammer, L.; Orpen, A. G.; Taylor, R. *J. Chem. Soc., Perkin Trans. 2* **1987**, S1−S19.

(18) Cotter, M. A. *J. Chem. Phys.* **1977**, *66*, 1098−106; *J. Chem. Phys.* **1977**, *67*, 4268−4270.

(19) Demus, D.; Hauser, A. In *Selected Topics in Liquid Crystal Research*; Koswig, H.-D., Ed.; Akademie-Verlag: Berlin, 1990; pp 19−44, and references therein.

Table 9. Electronic Polarizability and Quadrupolar Moments in Some 10- and 12-Vertex *p*-Carborane and Bicyclo[2.2.2]octane Derivatives[a]

		polarizability [Å^3]			quadrupole moments [D·Å]		
		$\alpha_{\|\|}$	Da	α_{avg}	$Q_{\|\|}$	ΔQ	Q_{avg}
			H−$\mathcal{A}$−H				
1[1]c	$\mathcal{A}$ = 1,12-$C_2B_{10}H_{10}$	108	−7	113	−71	11	−78
2[1]c	$\mathcal{A}$ = 1,10-$C_2B_8H_8$	96	1	95	−58	10	−64
3[1]c	$\mathcal{A}$ = 1,4-C_8H_{12}	74	0	74	−52	0	−52
			H−$\mathcal{A}$-$\mathcal{A}$−H				
1[2]c	$\mathcal{A}$ = 1,12-$C_2B_{10}H_{10}$	262	56	225	−139	21	−153
2[2]c	$\mathcal{A}$ = 1,10-$C_2B_8H_8$	232	59	192	−113	19	−126
3[2]c	$\mathcal{A}$ = 1,4-C_8H_{12}	167	33	145	−104	−1	−103
			HC≡C−$\mathcal{A}$−$\mathcal{A}$−C≡CH				
1[2]d	$\mathcal{A}$ = 1,12-$C_2B_{10}H_{10}$	373	160	267	−149	32	−170
2[2]d	$\mathcal{A}$ = 1,10-$C_2B_8H_8$	348	168	236	−127	26	−144
3[2]d	$\mathcal{A}$ = 1,4-C_8H_{12}	253	112	180	−127	−4	−124

[a] Obtained from HF/6-31G* calculations. Anisotropy defined as $\Delta X = X_{||} - X_{\perp}$.

Searching for other factors that may account for the mesogenic behavior of the molecules, we focused on quadrupole moments *Q* of the parent carboranes and their derivatives. Both carboranes have highly polarized C−B and B−H bonds, which give rise to substantial quadrupole moment tensors as compared to the less polarized bicyclo[2.2.2]octane system. This should lead to greater intermolecular interactions and to increase in melting and clearing temperatures for the carborane derivatives. Unfortunately, theoretical assessment of this effect on the nematic−isotropic transition is difficult, and typically multipoles are not treated by the theory of the nematic state.[20,21] We have demonstrated, however, that in two isosteric derivatives of 10-vertex cluster the quadrupolar interactions are significant and lead to a substantial stabilization of the nematic phase.[22] Also, an unusual stabilization of a smectic phase in a binary mixture can be attributed to quadrupolar interactions between the mixture components.[23]

An analysis of the computational results collected in Table 9 shows that the quadrupole moments calculated for 12-vertex carborane and its derivatives are larger by about 20% than those for the 10-vertex analogues and significantly larger (up to 50%) than those obtained for the bicyclo[2.2.2]octane derivatives. This coincides with the trend in melting temperatures in which the highest values are observed for the parent and two-ring 12-vertex carboranes **1[*n*]c** (Table 5). Despite a significant quadrupole moment in both 10-vertex derivatives, single- and two-cage carboranes **2[1]c** and **2[2]c** melt below the bicyclo[2.2.2]-octane analogues. Interestingly, the increase in melting temperature upon addition of a second cage to the parent compound is 95 °C for the 12-vertex carborane **1c**, 60 °C for bicyclo-[2.2.2]octane **3c**, and only 10 °C for the 10-vertex carborane **2c**. Such a modest increase in the melting temperature in the latter can be attributed to the significantly lower barrier to internal rotation around the C−C bond in the 10-vertex bi-*p*-carborane than the two other dimers (Table 4). It should be noted, however, that many other factors, including efficiency and type of packing, contribute to the melting transition, and these consideration can be used only in a qualitative way.[24]

It appears from the above discussion that the thermal behavior of 12-vertex carborane and bicyclo[2.2.2]octane is "normal", while that of the 10-vertex carborane is unexpected. The melting points, electronic polarizability, and quadrupole moments for **1c** and **3c** follow the same order, and the compounds also have similar barriers to internal rotation in the two-ring derivatives **1[2]c** and **3[2]c**. In the diheptyl derivatives, however, the trend is reversed and bicyclo[2.2.2]octane **3[2]a** clears significantly higher than the 12-vertex analogue **1[2]a**. This is presumably related to the significantly higher barrier to internal rotation around the alkyl−cage bond in the former relative to the analogous barrier in the 12-vertex derivative **1[2]a**, and hence higher conformational rigidity of the bicyclo[2.2.2]octane derivative. If this hypothesis is correct, then one can predict that the diheptynyl derivative of bicyclo[2.2.2]octane, **3[2]b**, should have a much lower virtual [T_i] than the 12-vertex analogue **1[2]b**. In this pair of compounds the conformational rigidity (or rather its lack) is similar in both compounds but **1[2]b** has a much higher quadrupole moment.

Overall, the results indicate that the mesogenic behavior is governed by a combination of steric (dynamic anisometry and conformational rigidity) and electronic factors (polarizability and multipolar moments). The generally good performance of bicyclo[2.2.2]octane as a mesogenic building block can be attributed to high barriers to internal rotation around the cage−substituent bond in its derivatives (high conformational rigidity) compared to those in the carboranes. Between the two *p*-carboranes, the 12-vertex cage is superior as a component of liquid crystal molecules due to more favorable conformational effects, higher overall electronic polarizability, and quadrupole moments. In the acetylenes **[2]b** there are no conformational effects and the difference in [T_i] can largely be attributed to differences in quadrupolar interactions.

Computational Methods

Ab initio calculations were carried out at the HF/6-31G* level of theory using the Gaussian 98 suite of programs[25] on an SGI R8000 workstation. Appropriate symmetry constraints were used in geometry optimizations. The ground-state conformations and transition states were verified by analysis of normal modes. Zero-point vibrational energies (ZPE) and thermodynamic properties at 298 K were calculated using the 0.9135 scaling factor.[26] The resulting energies are listed in the Supporting Information.

Nuclear magnetic shielding tensors were calulated for conformational minima using the NMR keyword and GIAO method

(20) Wojtowicz, P. J. In *Introduction to Liquid Crystals*; Priestly, E. B., Wojtowicz, P. J., Sheng, P., Eds.; Plenum Press: New York, 1975; pp 45−58.
(21) Madhusudana, N. V. In *Liquid Crystals: Applications and Uses*; Bahadur, B., Ed.; World Scientific: Singapore, 1990; Vol. 1, pp 38−90.
(22) Pakhomov, S.; Piecek, W.; Kaszynski, P. Submitted for publication.
(23) Czuprynski, K.; Douglass, A. G.; Kaszynski, P.; Drzewinski, W. *Liq. Cryst.* **1999**, *26*, 261−269.
(24) Ubbelohde, A. R. *The Molten State of Matter. Melting and Crystal Structure*; Wiley & Sons: New York, 1978.

at the HF/6-31G* level of theory. Hybridization was calculated using the NBO 3.1 subroutine in the Gaussian suite of programs.[27]

The electronic spectra for **2[2]d** and **2[2]c** were calculated using ZINDO (INDO/2, all electrons included in CI) in the Cerius2 suite of programs using the HF/6-31G*-optimized geometry.

Experimental Section

Melting points and enthalpies were measured with a TA Instruments DSC 2920 using a heating rate of 5 K min^{-1}. NMR spectra were obtained at the 400 MHz (^1H spectra), 75 MHz (^{13}C), or 128.4 MHz field (^{11}B) in $CDCl_3$ and referenced to TMS (^1H), $CDCl_3$ set at 77.0 ppm (^{13}C), or $B(OMe)_3$ set at 18.1 ppm (^{11}B). $^1H-^{13}C$ correlations were accomplished using the DEPT-135[28] and HMBC[29] experiments. IR spectra were recorded using thin films of sample deposited from CH_2Cl_2 solutions on NaCl disks. Mass spectrometry was performed using a Hewlett-Packard 5890 instrument (GCMS). Elemental analysis was provided by Atlantic Microlab, Norcross, GA. UV spectra were recorded in MeCN.

General Procedures for X-ray Crystallography.

A colorless crystal (approximate dimensions 0.42 × 0.24 × 0.21 mm for **1[2]a**, 0.40 × 0.25 × 0.25 mm for **1[2]b**, and 0.50 × 0.37 × 0.10 mm for **2[2]b**) was placed onto the tip of a 0.1 mm diameter glass capillary and mounted on a Siemens SMART system for data collection at 173 (2) K. A preliminary set of cell constants was calculated from reflections harvested from three sets of 20 frames. These initial sets of frames were oriented such that orthogonal wedges of reciprocal space were surveyed. This produced initial orientation matrices determined from 30 (for **1[2]a**), 43 for **1[2]b**) or 27 (for **2-[2]b**) reflections. Final cell constants were calculated from a set of 1441 (for **1[2]a**), 2789 for **1[2]b**) or 3032 (for **2[2]b**) strong reflections from the actual data collection.

Data for a colorless crystal of **2[2]a** (approximate dimensions 0.70 × 0.40 × 0.30 mm) were collected on a Rigaku AFC6S system at 193 (1) K at Vanderbilt University. The specimen was cut from a plate and coated with a mixture of mineral oil and grease. After the crystal was mounted on a glass fiber attached to a goniometer head, a microvial was placed over the crystal and fiber. The goniometer head was placed in a cooler and transported from the cold room (approximately 277 K) to the X-ray facility. The goniometer head was placed on the instrument and the vial was removed to attain a quickly frozen sample.

Preliminary cell constants for **2[2]a** and an orientation matrix for data collection were obtained from a least-squares refinement using the setting angles of 25 carefully centered reflections in the range $82.80 < 2\theta < 87.90$. The data were collected using the $\Omega\angle 2\theta$ scan technique to a maximum 2θ value of 120.2°. Omega scans of several intense reflections, made prior to data collection, had an average width at half-height of 0.42° with a takeoff angle of 6.0°. Scans of $(1.73 + 0.30 \tan(\theta))°$ were made at a speed of 16.0°/min (in Ω). The weak reflections ($I < 10.0\ \sigma(I)$) were rescanned (maximum of five rescans) and the counts were accumulated to ensure good counting statistics. Stationary background counts were recorded on each side of the reflection. The ratio of peak counting time to background counting time was 2:1. The diameter of the incident beam collimator was 1.0 mm, and the crystal-to-detector distance was 200.0 mm.

Relevant crystallographic data are given in Table 1.

The space group $P\bar{1}$ (for all four compounds) was determined based on systematic absences and intensity statistics. A successful direct-methods solution was calculated which provided all (for **1[2]a**) or most (for **1[2]b**, **2[2]a**, and **2[2]b**) non-hydrogen atoms from the E-map (SHELXTL-Plus V5.0, Siemens Inc., Madison, WI). For **1[2]b**, **2[2]a**, and **2[2]b** several full-matrix least squares/difference Fourier cycles were performed, which located the remainder of the non-hydrogen atoms. All non-hydrogen atoms were refined with anisotropic displacement parameters. All hydrogen atoms were placed in ideal positions and refined as riding atoms with relative isotropic displacement parameters.

One of the two substituents in **2[2]a** and **2[2]b** was disordered and 91 SHELXTL SAME, SADI, and SIMU restraints were applied to these groups to make them physically reasonable. These atoms were refined as isotropic atoms. All others were left as anisotropic. In **2[2]b** the atoms C(7)−C(9) in one of the heptynyl groups are disordered over two sites in a 73:27 ratio. Seventy-three bond length and anisotropic displacement restraints were applied to this group of atoms to make them to behave like the other pentyl chain in **2[2]b**.

1,1′-Bis[12-heptyl-1,12-dicarba-*closo*-dodecaborane] (1[2]a). *n*-Butyllithium (0.7 mL, 1.6 M in hexane, 1.12 mmol) was added to a solution of 1,1′-bis(1,12-dicarba-*closo*-dodecaborane) (**1[2]c**, 0.114 g, 0.4 mmol) in THF at −78 °C. The reaction mixture was stirred at ambient temperature for 20 min, and 1-iodoheptane (0.2 mL, 1.22 mmol) was added. After 2 h of stirring, the reaction mixture was filtered through a silica gel plug, which was washed with CH_2Cl_2. The solvent was evaporated, and the residue was sublimed (140 °C/0.1 Torr) and recrystallized (hexanes) to give 0.150 g (94% yield) of colorless crystals: ^1H NMR δ 0.0−3.0 (broad B−H absorption), 0.84 (t, J = 7.1 Hz, 6H), 1.0−1.1 (br m, 8H), 1.15−1.25 (br m, 12H), 1.48−1.52 (m, 4H); ^{13}C NMR δ 14.03, 22.53, 28.01, 29.00, 29.41, 31.62, 37.45, 78.27, 82.98; ^{11}B NMR δ −13.34 and −14.40 (d, J_{BH} = 149 Hz); IR 2632, 2606, 2589 cm^{-1}; EIMS, *m*/*z* 440−435 (max at 438, 15%), 426−422 (max at 424, 46%). Anal. Calcd for $C_{18}H_{50}B_{20}$: C, 44.78; H, 10.44. Found: C, 44.89; H, 10.36.

1,1′-Bis[12-hept-1-ynyl-1,12-dicarba-*closo*-dodecaborane] (1[2]b). *n*-Butyllithium (1.4 mL, 1.6 M in hexane, 2.24 mmol) was added to a solution of 1,1′-bis(1,12-dicarba-*closo*-dodecaborane) (**1[2]c**, 0.286 g, 1.0 mmol) in THF (15 mL) at −78 °C. The reaction mixture was stirred at ambient temperature for 20 min and then cooled to −78 °C, and vacuum-dried CuBr (0.35 g) was added. The mixture was stirred at ambient temperature for 30 min, and 1-bromohept-1-yne[30] (0.4 mL, about 2.3 mmol) was added. After overnight stirring, the reaction mixture was filtered through a silica gel plug, which was washed with hexanes. The solvent was evaporated, and the residue was sublimed (140 °C/0.1 Torr) and recrystallized (ethanol) to give 0.150 g (78% yield) of colorless crystals: ^1H NMR δ 0.0−3.0 (broad B−H absorption), 0.85 (t, J = 6.3 Hz, 6H), 1.20−1.30 (br s, 8H), 1.31−1.40 (m, 4H), 1.98 (t, J = 7.0 Hz, 4H); ^{13}C NMR δ 13.90, 18.37, 22.00, 27.57, 30.78, 68.51, 75.87, 78.99, 82.98; ^{11}B NMR δ −13.45 (d, J_{BH} = 163 Hz); IR 2614, 2251 cm^{-1}; UV, λ_{max} (log ϵ) 193.5 (4.71) nm; EIMS, *m*/*z* 472−477 (max at 475, 11), 457−462 (max at 460, 14), 442−450 (max at 446, 20). Anal. Calcd for $C_{18}H_{42}B_{20}$: C, 45.54; H, 8.92. Found: C, 45.62; H, 8.88.

1,1′-Bis[10-heptyl-1,10-dicarba-*closo*-decaborane] (2[2]a). It was prepared in a way analogous to that of **1[2]a**. Distilled product was recrystallized from ethanol and pentane (−78 °C) to furnish **2[2]a** in 87% yield: ^1H NMR δ 0.0−3.0 (broad B−H absorption), 0.93 (t, J = 6.4 Hz, 6H), 1.35−1.50 (br m, 12H), 1.51−1.58 (m, 4H), 1.94−2.02 (m, 4H), 3.23 (t, J = 8.3 Hz, 4H); ^{13}C NMR δ 14.13, 22.70, 29.19,

(25) Frisch, M. J.; Trucks, G. W.; Schlegel, H. B.; Scuseria, G. E.; Robb, M. A.; Cheeseman, J. R.; Zakrzewski, V. G.; Montgomery, J. A., Jr.; Stratmann, R. E.; Burant, J. C.; Dapprich, S.; Millam, J. M.; Daniels, A. D.; Kudin, K. N.; Strain, M. C.; Farkas, O.; Tomasi, J.; Barone, V.; Cossi, M.; Cammi, R.; Mennucci, B.; Pomelli, C.; Adamo, C.; Clifford, S.; Ochterski, J.; Petersson, G. A.; Ayala, P. Y.; Cui, Q.; Morokuma, K.; Malick, D. K.; Rabuck, A. D.; Raghavachari, K.; Foresman, J. B.; Cioslowski, J.; Ortiz, J. V.; Stefanov, B. B.; Liu, G.; Liashenko, A.; Piskorz, P.; Komaromi, I.; Gomperts, R.; Martin, R. L.; Fox, D. J.; Keith, T.; Al-Laham, M. A.; Peng, C. Y.; Nanayakkara, A.; Gonzalez, C.; Challacombe, M.; Gill, P. M. W.; Johnson, B. G.; Chen, W.; Wong, M. W.; Andres, J. L.; Head-Gordon, M.; Replogle, E. S.; Pople, J. A. *Gaussian 98*, revision A.7; Gaussian, Inc.: Pittsburgh, PA, 1998.
(26) Scott, A. P.; Radom, L. *J. Phys. Chem.* **1996**, *100*, 16502−16513.
(27) Glendening, E. D.; Reed, A. E.; Carpenter, J. E.; Weinhold, F. NBO version 3.1.
(28) Doddrell, D. M.; Pegg, D. T.; Bendall, M. R. *J. Magn. Reson.* **1982**, *48*, 323−327.
(29) Bax, A.; Summers, M. F. *J. Am. Chem. Soc.* **1986**, *108*, 2093−2094.
(30) 1-Bromo-1-heptyne (bp 56−7 °C/10 Torr; Straus, F.; Kollek, L.; Heyn, W. *Chem. Ber.* **1930**, *63*, 1937) was prepared from 1-heptyne according to a general procedure: Brandsma, L. In *Preparative Acetylenic Chemistry*; Studies in Organic Chemistry 34, 2nd ed.; Elsevier: New York, 1988; p 150.

29.64, 31.85, 31.99, 34.54, 112.60, 121.53; ^{11}B NMR δ −10.35 and −12.09 (d, $J_{BH} = 192_{avg}$ Hz); IR 2595 cm^{-1}; UV, λ_{max} (log ϵ) 200 (4.60) nm; EIMS, *m*/*z* 431−424 (max at 428, 16), 415−408 (max at 413, 30), 401−394 (max at 399, 38). Anal. Calcd for $C_{18}H_{46}B_{16}$: C, 49.64; H, 10.65. Found: C, 49.74; H, 10.56.

1,1′-Bis[10-hept-1-ynyl-1,10-dicarba-*closo*-decaborane] (2[2]b). It was prepared in a way analogous way to that of **1[2]b** in 81% yield: ^{1}H NMR δ 0.0−3.0 (broad B−H absorption), 0.95 (t, $J = 7.0$ Hz, 6H), 1.35−1.50 (m, 8H), 1.64−1.70 (m, 4H), 2.44 (t, $J = 7.0$ Hz, 4H); ^{13}C NMR δ 13.98, 19.21, 22.20, 28.11, 31.13, 77.00, 87.63, 102.2, 114.7; ^{11}B NMR δ −10.6 (d, $J_{BH} = 162$ Hz); IR 2605, 2360, 2342, 2251 cm^{-1}; UV, λ_{max} (log ϵ) 194 (4.35), 232 (4.75) nm; EIMS, *m*/*z* 425−431 (max at 428, 16), 409−415 (max at 412, 30), 394−401 (max at 398, 38). Anal. Calcd for $C_{18}H_{38}B_{16}$: C, 50.58; H, 8.96. Found: C, 50.64; H, 9.02.

Acknowledgment. We thank Drs. Mahesh K. Patel and Jadwiga Laska for their initial efforts to obtain single crystal data for **1[2]a** and **2[2]a**. This project has been supported in part by The Petroleum Research Fund (28742-G1) and the NSF CAREER grant (DMR-9703002).

Note Added after ASAP. There were errors in Table 5 in the version posted ASAP 11/06/2001; the corrected version was posted 11/07/2001.

Supporting Information Available: Four X-ray crystallographic files, in CIF format, listings of crystallographic coordinates for all four compounds, and full computational data including isotropic shielding tensors are available. Figure S1 showing thermal ellipsoid diagram representations of **1[2]a**, **1[2]b**, **2[2]a**, and **2[2]b**. This material is available free of charge via the Internet at http://pubs.acs.org.

IC010663X